Talanta 307 (2026) 129778

Contents lists available at ScienceDirect

Talanta

journal homepage: www.elsevier.com/locate/talanta

Fabrication and optimization of a hybrid 3D-printed flexible electrochemical biosensor for sensitive detection of 1-hydroxypyrene glucuronide, an associated wildfire exposure biomarker

Yonghao Fu [a,b], Chuchu Chen [a], Xinyi Li [a,b], Yang Song [a], Christopher D. Simpson [c], Luke P. Naeher [d], Kaiyan Qiu [a,*], Dan Du [a,b,**]

[a] School of Mechanical and Materials Engineering, Washington State University, Pullman, WA, 99164, United States
[b] Department of Pharmaceutical Sciences, College of Pharmacy and Pharmaceutical Sciences, Washington State University, Spokane, WA, 99202, United States
[c] Department of Environmental & Occupational Health Sciences, University of Washington, Seattle, WA, 98195, United States
[d] Department of Environmental Health Science, University of Georgia, Athens, GA, 30602, United States

ARTICLE INFO

Keywords:
3D printing
3D-printed electrochemical biosensor
1-Hydroxypyrene glucuronide
Wood smoke biomarker
Competitive immunoassay

ABSTRACT

The polycyclic aromatic hydrocarbons (PAHs) from wood smoke are harmful to human health. In this study, an innovative 3D-printed flexible electrochemical biosensor was developed for the detection of 1-hydroxypyrene glucuronide (1-OHPG), a major metabolite of PAHs in human urine. The proposed biosensor integrated competitive immunoassay and electrochemical analysis to enhance detection specificity and sensitivity. Three 3D printing techniques, fused deposition modeling (FDM), stereolithography (SLA), and direct ink writing (DIW), were synergistically combined to improve performance and reduce fabrication costs of the biosensor. Polylactic acid/carbon black-based electrodes were produced via FDM printing and activated through chemical treatment using N,N-dimethylformamide, 0.5 M H_2SO_4, 1 M NaOH followed by electrochemical treatment at 2.5 V for 100 s in 0.1 M PBS solution to enhance their electrochemical activity. The flexible biosensor substrate was fabricated using SLA printing to enable integration with the electrodes. Using the DIW method, Ag/AgCl conductive paste was printed to serve as the reference electrode. The hapten-bovine serum albumin conjugate was uniformly immobilized on the working electrode via DIW printing to enhance the sensitivity and selectivity of the bioassay. The biosensor exhibited a low detection limit of 0.012 ng/mL, a broad linear range from 0.01 to 200 ng/mL, and a recovery rate of 95% to 105% in spiked human urine samples. This study demonstrates a novel hybrid 3D-printed flexible biosensor for 1-OHPG detection in urine, offering a simple, accurate, sensitive and cost-effective strategy with great potential for rapid, portable and reliable biomonitoring of wood smoke exposure.

1. Introduction

Over the past several decades, both the area burned and the number of wildfires in the United States have increased rapidly, leading to a significant threat to lives and ecosystems [1,2]. According to data from the National Interagency Fire Center, 64,897 wildfires occurred in the United States in 2024, burning a total of 8,924,884 acres of land [3]. Firefighters are at high risk of adverse health effects due to frequent exposure to air pollutants released during wildfires [4,5]. Among these pollutants, polycyclic aromatic hydrocarbons (PAHs), which originate from the combustion of organic materials, are particularly hazardous [6,7]. In severe cases, exposure to PAHs has been shown to be highly toxic, mutagenic, carcinogenic, teratogenic, and immunotoxic to various life forms [5,8]. Therefore, to effectively protect firefighters' health, it is essential to monitor the biological impact of PAHs exposure in a rapid, efficient, accurate and cost-effective manner [9,10]. A common approach to assess exposure to PAHs and its impact on human health is the detection of PAH-derived metabolites in the body, such as S-phenylmercapturic acid (SPMA) [11], trans,*trans*-muconic acid (t,t-MA) [12], hippuric acid (HA) [13] and 1-hydroxypyrene glucuronide (1-OHPG) [14].

To measure 1-OHPG in urine, researchers have employed various

* Corresponding author.
** Corresponding author. School of Mechanical and Materials Engineering, Washington State University, Pullman, WA, 99164, United States.
E-mail addresses: kaiyan.qiu@wsu.edu (K. Qiu), annie.du@wsu.edu (D. Du).

https://doi.org/10.1016/j.talanta.2026.129778
Received 29 December 2025; Received in revised form 19 March 2026; Accepted 4 April 2026
Available online 6 April 2026
0039-9140/© 2026 Elsevier B.V. All rights are reserved, including those for text and data mining, AI training, and similar technologies.

methods, including ultra-performance liquid chromatography-tandem mass spectrometry (UPLC-MS/MS) [15], high-performance liquid chromatography (HPLC) [16], gas chromatography-mass spectrometry (GC-MS) [17], and liquid chromatography–tandem mass spectrometry (LC-MS/MS) [16,18], leading to significant progress in the monitoring of 1-OHPG. These chromatographic techniques offer several advantages, including high sensitivity, good selectivity, strong versatility and superior separation efficiency, enabling accurate qualitative and quantitative analysis of trace-level biomarkers in complex biological matrices [19]. However, despite their strong analytical performance, these methods still face practical limitations in routine and rapid on-site analysis. For instance, HPLC analysis typically requires 2-16 h of enzymatic hydrolysis and sample extraction prior to detection, which greatly reduces overall efficiency [20]. The influence of incomplete hydrolysis on analytical results must also be considered [21]. Similarly, derivatization steps are often required in LC-MS/MS and GC/MS to improve detection accuracy, further constraining their applicability for on-site rapid 1-OHPG detection [17,18]. The expensive large-scale analytical equipment also greatly increases the cost of detection [22]. Obviously, there is a lack of simple, rapid, accurate and cost-effective detection methods for on-site detection of 1-OHPG. In recent years, electrochemical biosensors have emerged as a promising alternative, offering rapid, accurate, and sensitive responses for biomarker detection [23,24]. Their fast analysis time, simple instruments, ease of miniaturization, portability and low cost effectively address the limitations associated with traditional methods [25–27]. Building on these advantages, we have also developed multiple electrochemical biosensors for the detection of various biomarkers, such as glucose, uric acid, $A\beta_{1\text{-}42}$, atrazine, and acetochlor, for monitoring human health and disease diagnosis [28–31].

Three-dimensional (3D) printing has rapidly emerged as a popular approach for developing electrochemical sensors in recent years [32–37]. 3D printing offers significant advantages over traditional manufacturing methods, including low cost, material versatility, geometric flexibility, and compatibility with fluidic devices [38–41]. Commonly used 3D printing techniques include fused deposition modeling (FDM), stereolithography apparatus (SLA), and direct ink writing (DIW) [42,43]. FDM is currently the most widely used 3D printing method due to its ease of use, rapid production and low cost [44]. The fabrication of electrodes used in electrochemical biosensors is a popular application for FDM [45]. In this application, polylactic acid (PLA) and acrylonitrile butadiene styrene are blended with various carbon allotropes to create carbon composite filaments, which can be easily printed into customized electrode geometries for practical electrochemical sensing applications [44,46–48]. SLA is a high-resolution 3D printing technique that offers superior printing accuracy and excellent surface quality, both of which are critical for precise sensor fabrication [42]. In particular, flexible resin printed via SLA has been widely applied in the fabrication of flexible biosensors [49]. Meanwhile, DIW is a versatile 3D printing technique capable of processing diverse materials including hydrogel, polymer and nanocomposites [32,42]. Our group has successfully applied this technique to the fabrication of flexible and wearable devices as well as organ models [41,50]. Additionally, conventional surface modification of electrochemical biosensors commonly relies on drop-casting. However, this method often suffers from the coffee ring effect, poor reproducibility, and uneven biomolecule distribution on small electrodes [51,52]. To address these limitations, DIW was employed for the controlled deposition of biomolecules on the 3D-printed electrodes due to its precise spatial control and programmable dispensing capability. Our previous work demonstrated the feasibility of DIW for enzyme immobilization [32], and in this study the strategy is extended to the controlled deposition of hapten-bovine serum albumin (BSA) conjugates for immunosensor fabrication.

Herein, we developed a novel and sensitive detection approach using a 3D-printed flexible electrochemical biosensor for 1-OHPG detection in human urine. The recognition of 1-OHPG was based on a competitive immunoassay, in which the 1-OHPG in sample competed with the hapten-BSA conjugates immobilized on the electrode surface for a limited amount of anti-1-OHPG antibody (Ab) in the buffer solution. Subsequently, the polyclonal sheep anti-1-OHPG Ab was captured by donkey anti-sheep immunoglobulin G (IgG) labeled with the horseradish peroxidase (HRP), which catalyzed the reaction between hydrogen peroxide (H_2O_2) and thionin acetate (TA) to generate an electrochemical signal. The proposed approach offers several advantages. First, the FDM printing technique enables straightforward fabrication of the electrodes, significantly reducing costs while improving production efficiency. Second, the use of SLA with flexible resin provides high printing resolution and mechanical robustness, while the resulting substrate flexibility facilitates integration with electrodes. Third, the DIW printing technique enables precise immobilization of the hapten-BSA conjugate on the electrode surface, improving detection stability and accuracy. In addition, the immunochemical reaction-based design ensures selectivity and specificity. Finally, electrode surface modification enhances the electrochemical properties of the 3D-printed electrodes, thereby increasing sensitivity.

2. Experimental section

2.1. Chemicals and materials

Sheep anti-1-OHPG Ab and hapten-BSA conjugate were obtained from Chemitrace Consultancy (Natland, United Kingdom). Tween-20, phosphate-buffered saline (PBS), donkey anti-sheep IgG, HRP, sulfuric acid (51% w/w), hydrogen peroxide (30 wt%), N,N-dimethylformamide (DMF), potassium ferricyanide (III), TA, and silver/silver chloride (Ag/AgCl) paste were bought from Sigma-Aldrich Chemical Co. (St. Louis, MO, USA). Sodium hydroxide, potassium hexacyanoferrate (II) trihydrate were bought from Thermo Fisher Scientific Inc. (Waltham, MA, USA). Electrically conductive composite PLA filament (CDP11705) was bought from Protoplant (Vancouver, WA, USA).

2.2. Fabrication of 3D-printed flexible electrochemical 1-OHPG biosensor

3D printing was performed on Ender-3 Pro FDM printer (Creality, Hong Kong) using PLA/carbon black (CB) filament (Protopasta, Vancouver, WA, USA) to fabricate the working electrode (WE) and counter electrode (CE). The nozzle and bed temperatures were set to 210 °C and 60 °C, respectively. The electrode was fabricated with an infill density of 100%, a printing speed of 40 mm/s, and a horizontal orientation, with the working surface parallel to the build platform (X–Y plane). The sensor substrate (2 cm × 1.5 cm) with three slots (WE, CE and RE slot) was printed using Form 3+ printer (Formlabs, Somerville, MA, USA) with Flexible 80A V1 resin (Formlabs, Somerville, MA, USA). The WE and CE were integrated into the respective slots on the sensor substrate and sealed by silicone sealant (LOCTITE SI 595 clear RTV silicone adhesive sealant) to ensure only the activated electrode surface was exposed to the detected solution. Afterwards, the reference electrode (RE) was printed into the slot of the same substrate using Ag/AgCl paste via the DIW method (customized 3D-printing system with 3 Z-axis stages, Aerotech AGS 1000) to complete the biosensor.

2.3. Preparation of activated 3D-printed electrodes

The 3D-printed PLA/CB WEs were immersed in the DMF solution for 5, 10 and 20 min to prepare the DMF-activated electrodes. Similarly, the electrodes were immersed in 0.5 M diluted sulfuric acid and 1 M NaOH solution for 30, 60 and 180 min to prepare H_2SO_4-activated and NaOH-activated electrodes, respectively. In addition, the electrodes were immersed into the above three solutions in sequence to prepare the DMF/NaOH/H_2SO_4-activated electrodes. For the electrochemical activation procedure, the electrodes were immersed in 0.1 M PBS solution (pH 7.2), and constant voltages of 1.5, 2, and 2.5 V were first applied to the electrodes using a CHI660E electrochemical workstation (CH

Instruments, Austin, TX, USA) to determine the optimal activation potential. After identifying 2.5 V as the optimal condition, different activation times (50, 100, 150 and 200 s) were further investigated at this potential to prepare electrochemical-activated electrodes. Following activation, the electrochemical performance of the electrodes was evaluated by cyclic voltammetry (CV) in the 5 mM $[Fe(CN)_6]^{4-/3-}$ solution with 0.1 M KCl as the supporting electrolyte at a scan rate of 50 mV/s.

2.4. Immobilization of hapten-BSA conjugate on the WE surface

The hapten-BSA conjugate was immobilized on the WE by the drop casting and DIW methods, respectively. A total of 4 μL of 50 ng/μL hapten-BSA conjugate was slowly dropped onto the WE surface using a pipette. By adjusting the nozzle pressure and printing time, the same volume of hapten-BSA conjugate was printed onto the WE via the DIW method. The DIW process followed a circular path, with a set pressure of 10 kPa and a printing time of 4 s. The DIW process is shown in Movie S1 of the supplementary information. After drying at room temperature, the WEs prepared by the two methods were obtained.

Supplementary video related to this article can be found at https://doi.org/10.1016/j.talanta.2026.129778.

2.5. Characterization of 3D-printed electrodes

The 3D-printed electrodes, including original electrode (without hapten-BSA conjugate immobilization), the drop casting-immobilized electrode, and the DIW-immobilized electrode, were mounted onto scanning electron microscopy (SEM) stubs using carbon adhesive tabs. A thin layer of Au (10 nm) was then sputter-coated onto the samples to ensure high-quality image acquisition and to prevent charging under the electron beam during high-voltage, high-vacuum SEM imaging. The SEM imaging was performed using the FEI Quanta 200F SEM, equipped with a field emission gun electron source and a high-resolution secondary electron detector, operating in high vacuum. To obtain high-quality images with sufficient detail, the SEM measurements were taken at an accelerating voltage of 20 kV, a working distance of 9.2 mm, and a scan speed of 30 μs, with a spot size of 3 for the electron beam.

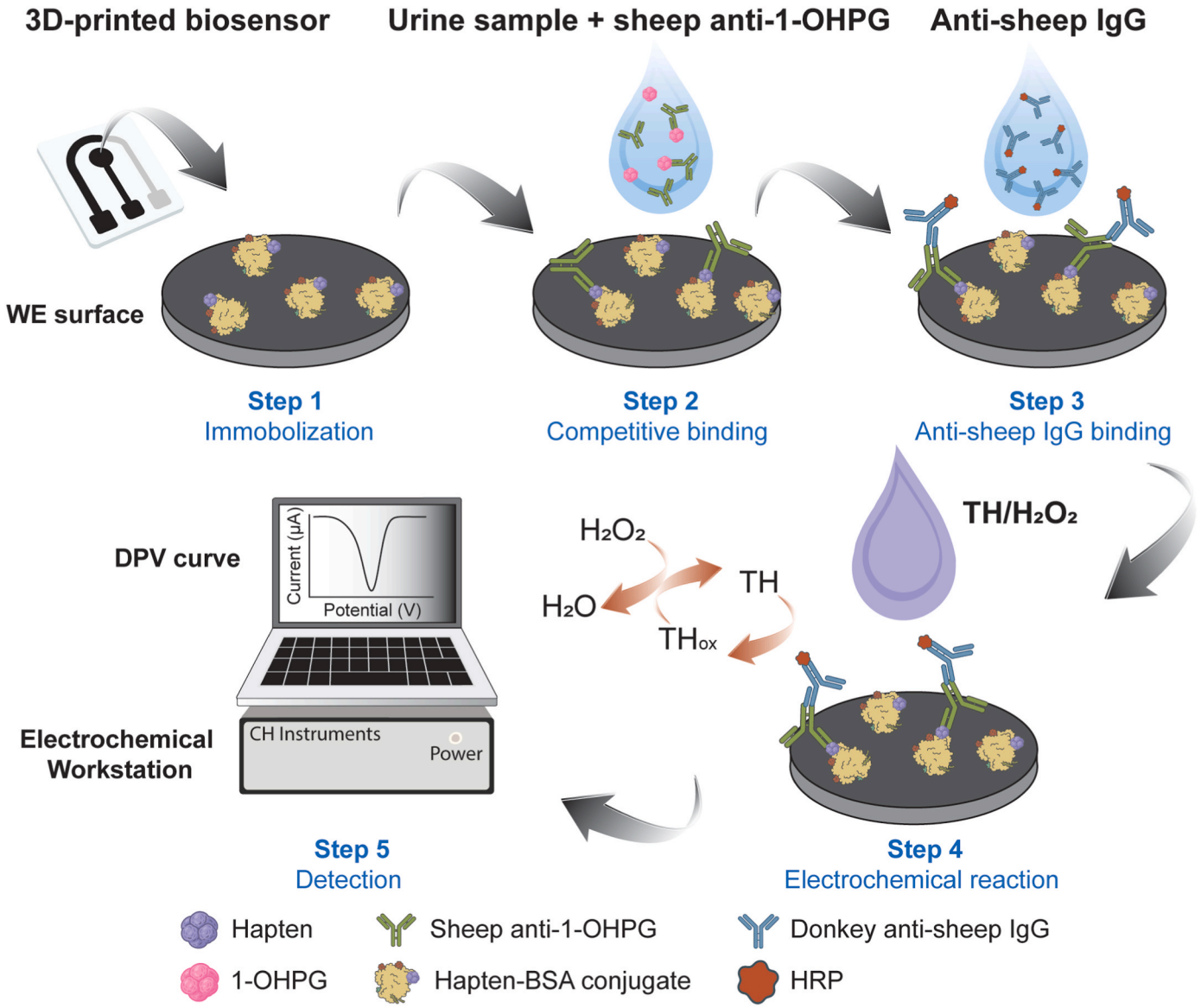

Fig. 1. Detection mechanism of the 3D-printed flexible electrochemical biosensor for 1-OHPG. IgG: Immunoglobulin G; BSA: Bovine serum albumin; HRP: Horseradish Peroxidase; TH: Thionine. THox: Oxidized thionine; DPV: Differential pulse voltammetry. WE: Working electrode.

2.6. Detection procedure of 3D-printed flexible electrochemical 1-OHPG biosensor

After drying at room temperature, the hapten-BSA conjugate-immobilized WEs were washed three times with PBST buffer (0.05% TWEEN-20 in PBS). After drying, 10 μL of PBST buffer containing 1% BSA was dropped onto the WE surface for blocking at 37 °C for 1 h. Afterwards, the WEs were washed three times again with PBST buffer. The anti-1-OHPG Ab was mixed with various concentrations of 1-OHPG to prepare the detection solution. Then, 5 μL of the detection solution was added onto the WE surface and incubated at 37 °C for 2 h. Subsequently, the WEs were washed three times with PBST. After connecting the biosensor to the electrochemical workstation, 50 μL of a solution containing 1 mM thionin acetate and 50 mM hydrogen peroxide was added to fully cover all three electrodes. Finally, the electrochemical signal was recorded using an electrochemical workstation to obtain the differential pulse voltammetry (DPV) curves.

3. Results and discussion

3.1. Principle of the 3D-printed flexible electrochemical 1-OHPG biosensor

The principle of the 3D-printed flexible electrochemical immunoassay biosensor is illustrated in Fig. 1. First, hapten-BSA conjugate ink was printed onto the WE using DIW method to immobilize the hapten-BSA conjugates on the WE surface (Step 1). The sheep anti-1-OHPG Ab solution was mixed with the sample containing 1-OHPG to allow binding, and the resulting mixture was then dropped onto the WE surface. Unbound sheep anti-1-OHPG Abs subsequently bound to the immobilized hapten-BSA conjugates on the WE surface, whereas the complexes of 1-OHPG and anti-1-OHPG were unable to bind (Step 2). In other words, the 1-OHPG in the sample competed with the hapten-BSA conjugates for binding to anti-1-OHPG Abs. Afterwards, donkey anti-sheep IgG bound to the sheep anti-1-OHPG Abs, with its HRP conjugate also immobilized on the electrode surface (Step 3). HRP catalyzed the oxidation of thionine to its oxidized form, thionine (ox), in the presence of H_2O_2, generating a peak in the DPV curve [29] (Step 4). In this process, more HRP resulted in more thionine (ox), which in turn produced a higher current reduction peak in the DPV recorded by electrochemical workstation (Step 5). Therefore, the concentration of 1-OHPG in the samples was inversely proportional to the peak current observed in the DPV curve.

3.2. Fabrication of 3D-printed flexible electrochemical 1-OHPG biosensor

The 3D-printed flexible electrochemical biosensor was fabricated by a strategy employing multiple 3D printing techniques (Fig. 2), wherein each printing technique was selected to meet the corresponding functional requirements of the biosensor components.

To achieve the desired function of the 1-OHPG electrochemical biosensor, the WE and CE of the biosensor should possess high electrical conductivity, durability and mechanical strength, while remaining cost-effective [53,54]. To meet these requirements, we selected PLA/CB filament and employed FDM method to fabricate the WE (reaction area: 2 mm) and CE, as shown in Fig. 2. The primary advantage of this approach is that FDM enables the use of conductive polymer composites, where PLA ensures mechanical stability and ease of printing, while CB enhances electrical conductivity, producing electrodes with electrochemical performance for sensing applications [53,55–57]. In addition, the surface of PLA-based electrodes can be chemically or electrochemically modified and activated to increase electroactive surface area, improving sensing performance [58,59].

For the sensor platform, a flexible and high-resolution substrate is required to integrate the electrodes effectively. Therefore, SLA printing with a flexible resin was employed to fabricate the miniature substrate (2 cm × 1.5 cm), as shown in Fig. 2. Through precise printing resolution, slots were printed on the substrate to match the size of the electrodes for assembling the WE and CE. Besides, the smooth surface also facilitates electrode attachment ensuring improved sealing and adhesion. Finally, the flexibility of resin provides mechanical compliance, enabling device bending without loss of structural integrity [60], and paving the way for future wearable sensor applications.

The reference electrode requires high stability, a well-defined potential, reproducibility, and compatibility with the platform. For this, we used DIW printing to directly deposit Ag/AgCl conductive paste, a well-

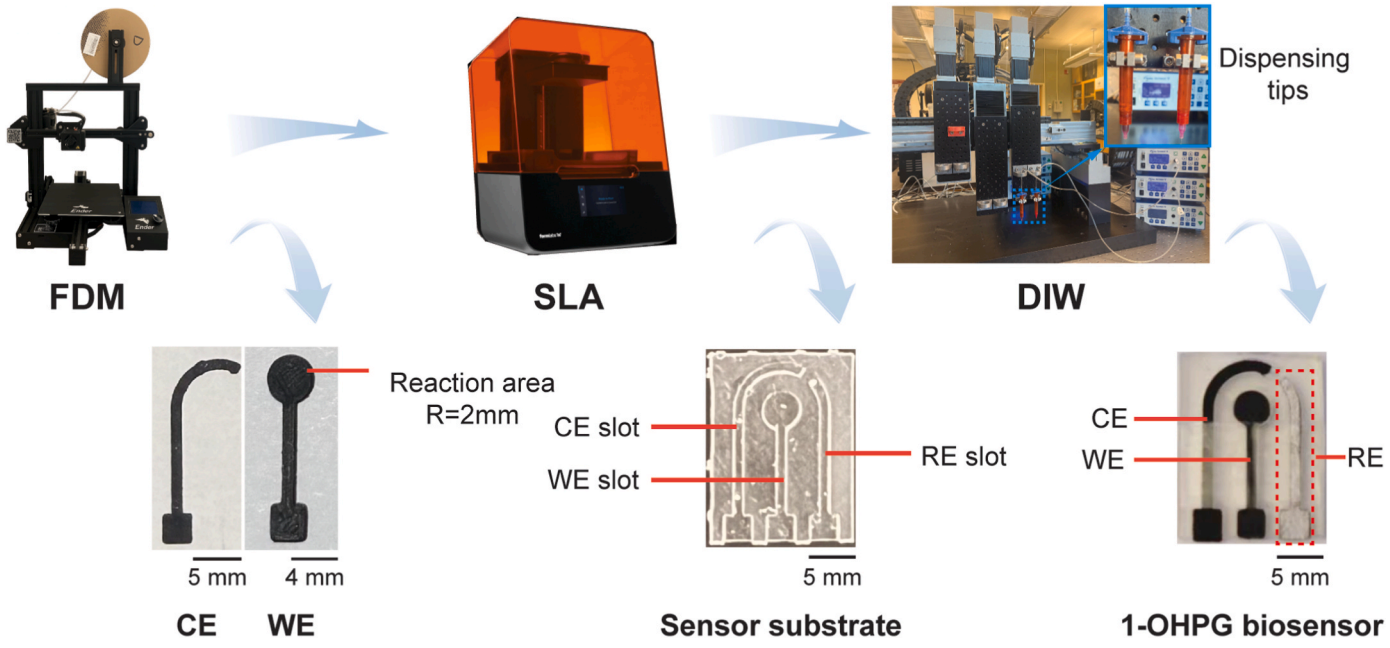

Fig. 2. Fabrication of 3D-printed flexible electrochemical 1-OHPG biosensor. FDM: fused deposition modeling; SLA: stereolithography apparatus; DIW: direct ink writing; WE: working electrode; CE: counter electrode; RE: reference electrode. The top-right blue box shows a magnified view of the dispensing tips and needles of the DIW system. The DIW-printed Ag/AgCl reference electrode is highlighted within the dotted box in the 1-OHPG biosensor image.

established reference material with a stable potential in an aqueous environment [61], via our customized 3D-printing system (AGS 1000, Aerotech) with 3 Z-axis stages, as shown in Fig. 2. The dispensing tip loaded with Ag/AgCl conductive paste is marked by a blue dotted box, with an enlarged view shown in the top-right blue box in Fig. 2. DIW enables precise deposition of Ag/AgCl paste into defined geometries (shown in the red dotted box in Fig. 2), producing reproducible reference electrodes [62]. Unlike other methods, DIW with Ag/AgCl paste avoids high-temperature curing [42], preserving the integrity of flexible resin substrate and FDM-printed WE and CE.

By combining FDM for conductive electrodes, SLA for flexible structural support, and DIW for reproducible reference electrodes, this hybrid approach achieved the fabrication of a fully integrated electrochemical sensor with mechanical flexibility, stable performance and cost-efficient production. In addition to its fabrication advantages, the proposed platform also offers low material cost. The estimated material cost of each sensor is approximately $0.17, which is lower than that of conventional gold electrodes and commercial screen-printed electrodes.

3.3. Activation of 3D-printed PLA/CB electrodes

Exposing the active carbon-based materials on the electrode surface can effectively improve the electrochemical performance of 3D-printed PLA electrodes [63]. The organic solvent DMF can dissolve the PLA, thereby exposing the electrochemically active sites [56]. Selective removal of PLA by NaOH-induced saponification is also a common chemical activation method [64,65]. Moreover, acid treatment can introduce oxygenated groups, including carboxyl and hydroxyl groups, to improve the hydrophilicity of electrode surface [66,67]. Kalinke et al. reported that activation with H_2SO_4 generated more oxygenated groups on the electrode surface than with HNO_3 activation due to the stronger oxidizing capacity of H_2SO_4 [63]. Therefore, DMF, NaOH and H_2SO_4 were used for chemical activation to enhance the electrochemical activity of electrode surface in this study. The redox couple $[Fe(CN)_6]^{4-/3-}$ was used as a probe to assess the electrochemical behavior and surface activation of electrodes, as it is highly sensitive to changes on carbon-based electrodes [54]. As shown in Fig. 3, the CV responses of 3D-printed electrodes treated with different activation methods were evaluated with respect to the $[Fe(CN)_6]^{4-/3-}$ redox probe. The original electrode exhibited poor electrochemical activity because the carbon active sites were blocked by PLA matrix, resulting in the absence of redox peak in the CV curve (black line in Fig. 3). The effects of different immersion times for DMF, NaOH and H_2SO_4 are shown in Fig. 3A, B and C, respectively. A smaller peak-to-peak separation between oxidation and reduction peaks indicates improved electrochemical performance [68]. For DMF treatment, the 10 min-treatment yielded the best performance (blue line in Fig. 3A). Longer treatment times resulted in diminished performance due to excessive PLA removal, which degraded the electrode structure, as observed in the 20-min treatment. For NaOH, the optimal activation time was 60 min (blue line in Fig. 3B), among the treatment durations of 30, 60 and 180 min H_2SO_4 activation showed a relatively modest effect, with a similar peak-to-peak separation observed for 60 min (blue line in Figs. 3C) and 180 min (green line in Fig. 3C) treatments, although the latter produced a higher current density. As shown in Fig. S1, the electrodes subjected to the combined treatment with DMF, NaOH and H_2SO_4 exhibited a smaller separation between peaks and higher current response compared with electrodes treated with a single treatment. These results indicate improved electron-transfer kinetics and enhanced electrochemical activity after the combined activation process. Based on these findings, the chemical activation times were selected as 10 min for DMF, 60 min for NaOH, and 180 min for H_2SO_4 in subsequent experiments.

Electrochemical activation parameters were further optimized (Fig. 3D and E), as previous studies have demonstrated that electrochemical activation plays a crucial role in enhancing electrochemical performance [54,69]. First, different activation potentials were

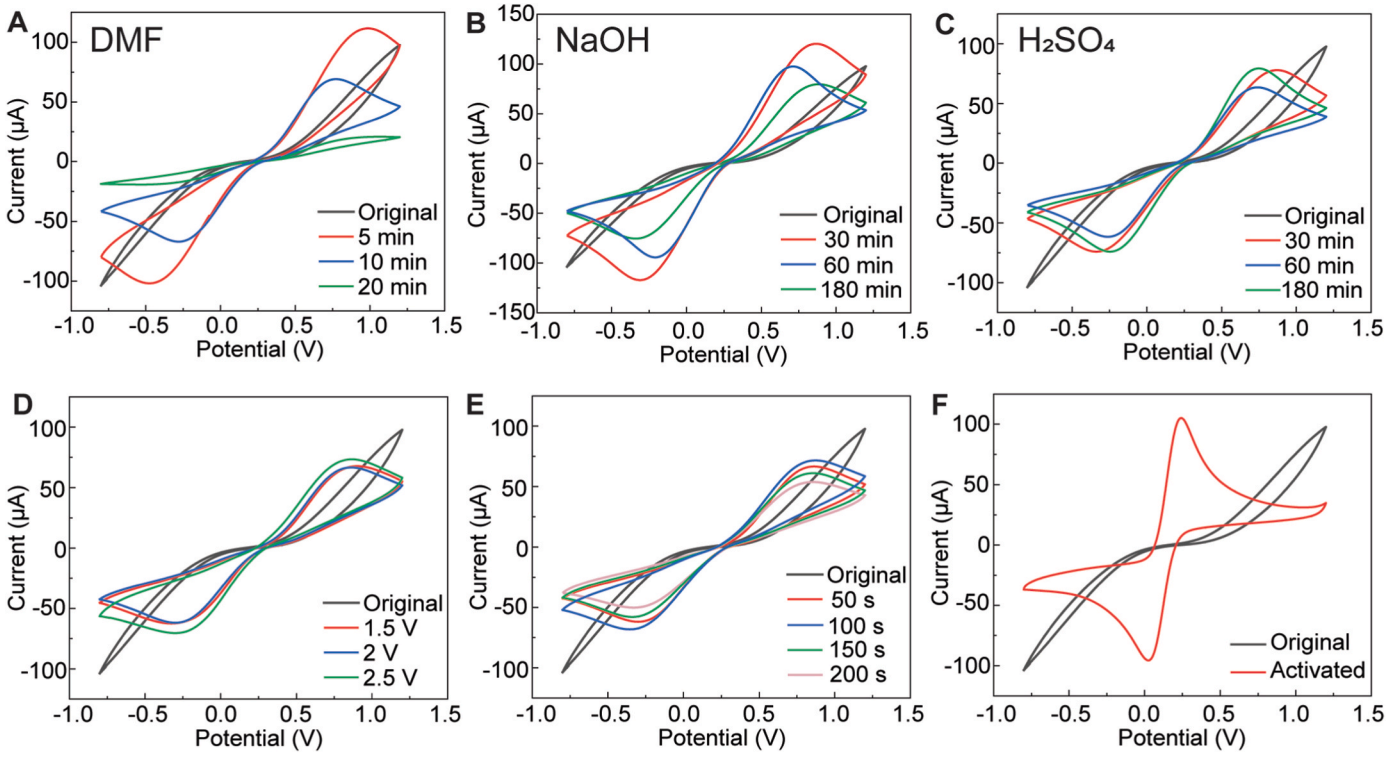

Fig. 3. CV curves of the WE after different activation methods, recorded in a 5 mM $[Fe(CN)_6]^{4-/3-}$ solution with 0.1 M KCl as the supporting electrolyte at a scan rate of 50 mV/s. (A) Effect of DMF treatment. (B) Effect of NaOH treatment. (C) Effect of H_2SO_4 treatment. (D) Effect of applied potential during electrochemical activation. (E) Effect of electrochemical activation time. (F) Comparison of the WE before and after all activations. The activation process involved chemical treatments with DMF (10 min), NaOH (60 min), and H_2SO_4 (180 min), followed by electrochemical activation at a potential of 2.5 V for 100 s.

evaluated, and 2.5 V (green line in Fig. 3D) was identified as the optimal potential, as it produced the smallest peak-to-peak separation in the CV curves, indicating improved electron transfer kinetics. Subsequently, the activation time was optimized under this potential (2.5 V). As shown in Fig. 3E, an activation time of 100 s (blue line) provided the best electrochemical performance. Electrochemical activation was then carried out at 2.5 V for 100 s in subsequent experiments. After all activation steps, CV measurement was performed in a 5 mM $[Fe(CN)_6]^{4-/3-}$ solution with 0.1 M KCl as the supporting electrolyte at a scan rate of 50 mV/s, and the resulting curve is presented in Fig. 3F. Compared to the original electrode (black line), the activated electrode (red line) exhibits well-defined oxidation and reduction peaks with a small peak-to-peak separation of approximately 100 mV, indicating enhanced electrochemical performance. Previous studies have reported electrochemical activation at lower potentials in alkaline or acidic media, which may offer greener alternatives to solvent-assisted activation [65,70]. In this work, the selected activation protocol was adopted because it provided reliable and reproducible electrochemical performance for the printed PLA/CB electrodes. Further optimization toward greener activation conditions will be explored in future work.

3.4. Immobilization of hapten-BSA conjugate on working electrode

The drop-casting method is widely used for surface modification of the WE in electrochemical biosensors [51,52]. Although drop-casting is simple to operate, its drawbacks, such as the coffee ring effect (CRE), low reproducibility and uneven distribution, can negatively impact biosensor performance [71]. The coffee ring effect refers to the phenomenon in which a ring-like stain forms after a droplet containing non-volatile particles dries. As the liquid evaporates, the edge of the droplet stays pinned, causing a flow that carries the particles to the outer edge, leaving a concentrated ring [72]. Obviously, CRE leads to an uneven distribution of the deposited materials on the WE surface. To address this limitation, we used DIW technique to print the hapten-BSA conjugate on the 3D-printed WE of the biosensor. Fig. 4 compares the DIW and drop-casting methods for preparing the hapten-BSA conjugate-immobilized electrodes and illustrates the process of both immobilization techniques. For the drop-casting method, 4 μL of hapten-BSA conjugate was manually dropped onto the WE surface using a pipette. However, the limited electrode surface area and the trace amount of addition hinder the uniform distribution of hapten-BSA conjugate, reducing the reproducibility of electrodes, thereby affecting the sensitivity and accuracy of detection. The DIW method is shown in Movie S1 of the supplementary information. The pump pressure was set to 10 kPa and the print time to 4 s for the DIW printer, allowing precise printing of 4 μL of hapten-BSA conjugate ink onto the WE surface. As shown in Fig. 4A, the starting position of DIW is marked with a red dot, and the DIW path is a circle, unlike the drop-casting method, which deposits only at the center of the electrodes.

To compare the effects of the two methods for immobilizing the hapten-BSA conjugates, SEM was used to observe the electrode surface. The original WE surface after multiple activations is shown in Fig. 4B. Compared to the original surface, the hapten-BSA conjugates were immobilized on the surface of WE, as shown in Fig. 4B and C. The distribution of hapten-BSA conjugates on the WE surface prepared by DIW method is more uniform than that produced by the drop-casting method.

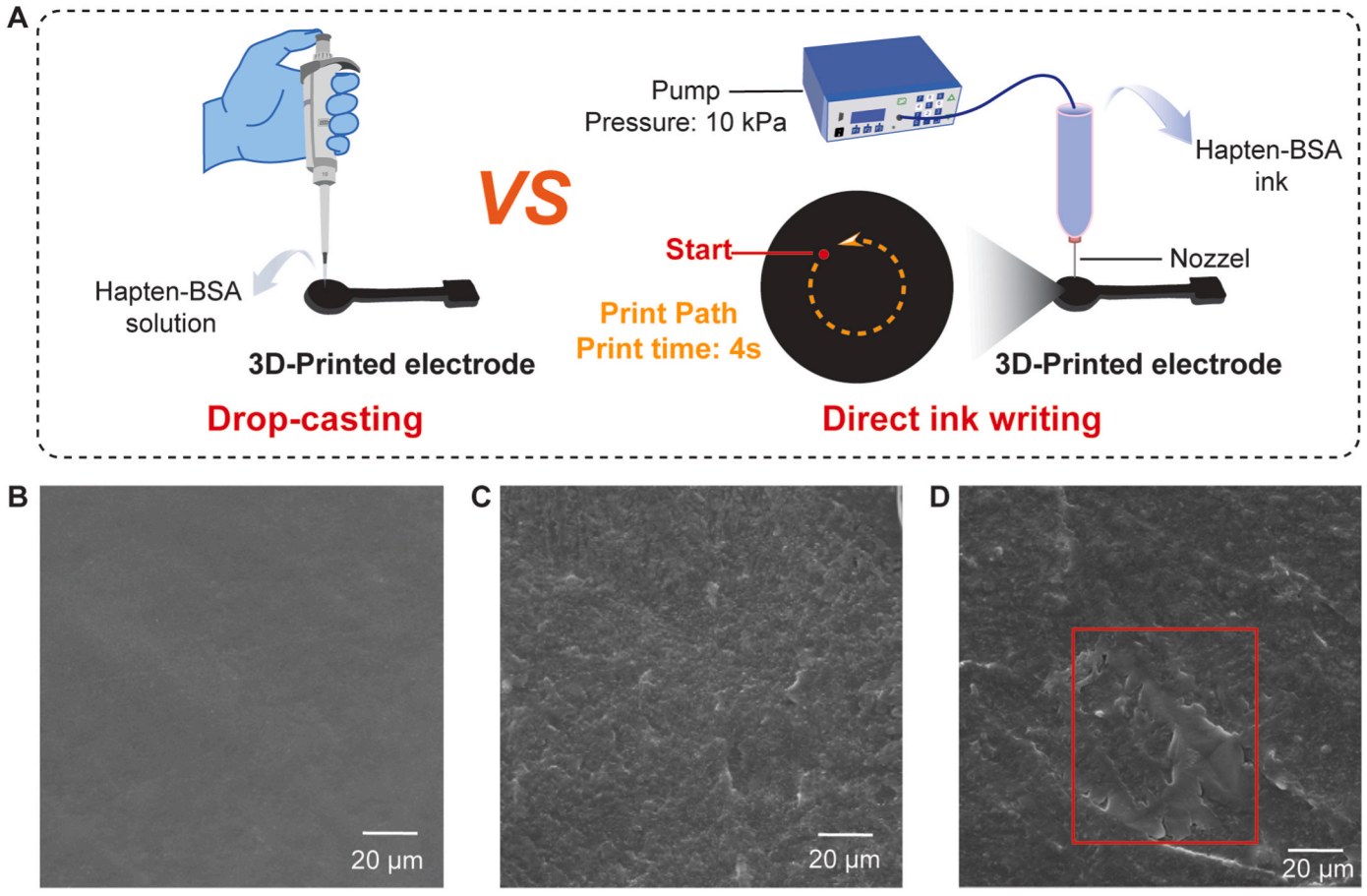

Fig. 4. Comparison of DIW and drop-casting immobilization methods. (A) The schematic illustration of two immobilization methods. **(B)** SEM image of the WE surface without hapten-BSA conjugate immobilization. **(C)** SEM image of the WE surface with hapten-BSA conjugate immobilized using the DIW method. **(D)** SEM image of the WE surface with hapten-BSA conjugate immobilized using the drop-casting method. The red box shows the aggregation of the hapten-BSA conjugates on the WE surface.

In addition, the aggregation of hapten-BSA conjugates can be observed on the surface of the drop-casting WE (red box in Fig. 4D). The uniform immobilization of hapten-BSA conjugates is mainly due to DIW's ability to dispense hapten-BSA conjugate ink from a nozzle in the millimeter-to micrometer-scale range and deposit it with a high level of spatial control and precision [32]. Meanwhile, the nozzle moves in a circular trajectory to evenly print the ink on the WE surface, ensuring the even distribution of hapten-BSA conjugate (Fig. 4A and Movie S1). By setting the printing speed and pressure, the dispensed volume of ink can be accurately controlled, offering a higher accuracy than the manual drop-casting method and thereby improving the reproducibility of electrode fabrication. In summary, the DIW method significantly avoids the uneven distribution caused by CRE in drop-casting, which improves the distribution of immobilized hapten-BSA conjugate on the WE surface, and thereby will enhance the detection performance of the biosensor.

3.5. Optimization of 1-OHPG detection conditions for the 3D-printed flexible electrochemical biosensor

Six crucial conditions influencing the immunoassay performance were optimized: the amount of hapten-BSA conjugates, dilution of sheep anti-1-OHPG Abs, dilution of donkey anti-sheep IgG, incubation time, buffer pH and test duration, as shown in Fig. 5. The DPV peak current was employed to represent the signal strength generated by the 1-OHPG biosensor. As illustrated in Fig. 5A, the peak current significantly increased with the amount of hapten-BSA conjugates immobilized on the WE surface, rising from 80 ng to 200 ng. Beyond 200 ng, the current plateaued, indicating saturation of the binding sites. For the sheep anti-1-OHPG Ab (Fig. 5B), the peak current increased with dilution factor from 3000 to 5000, with no statistically significant variation observed at higher dilutions. Similarly, the peak current intensity increased with the dilution factor of donkey anti-sheep IgG from 200 to 1000, with the highest current observed at a dilution factor of 1000, beyond which further dilution resulted in no appreciable change, as shown in Fig. 5C. In Fig. 5D, the incubation time was extended from 30 to 180 min, with the peak current reaching a maximum at 120 min. No further enhancement was observed beyond 120 min, suggesting equilibrium binding had been achieved. The effect of buffer pH on detection performance is displayed in Fig. 5E, where the optimal current response was obtained at pH 7. Deviations from this pH, either more acidic or more basic, led to diminished peak current intensity. Finally, the optimal test time was determined to be 2 min as shown in Fig. 5F. The above optimal conditions were applied to the subsequent 1-OHPG biosensing process.

3.6. Detection performance of 3D-printed flexible electrochemical 1-OHPG biosensor

The analytical performance of the 3D-printed flexible electrochemical 1-OHPG biosensor is shown in Fig. 6. It was evaluated by measuring samples containing varying concentrations of 1-OHPG. As shown in Fig. 6A, the DPV curves corresponding to different 1-OHPG concentrations ranging from 0.005 to 500 ng/mL were recorded. The peak currents were observed within the potential window of −0.25 V to −0.2 V. The peak current decreases with increasing 1-OHPG concentrations, consistent with the proposed detection mechanism. As illustrated in Fig. 6B, a linear relationship was established between the peak current and the logarithm of the 1-OHPG concentration. The biosensor exhibits a linear detection range from 0.01 ng/mL to 200 ng/mL, described by the regression equation I = −6.94 log (Conc. of 1-OHPG) + 21.6, with a coefficient of determination (R^2) value of 0.983. Based on the signal-to-noise ratio of 3 (S/N = 3), the limit of detection (LOD) is calculated to be 0.012 ng/mL. The enhanced sensitivity can be attributed to the improved electrochemical activity of the 3D-printed PLA/CB working electrode after chemical and electrochemical activation, which increases the electroactive surface area and facilitates electron transfer. In addition, the DIW printing of hapten-BSA enables uniform

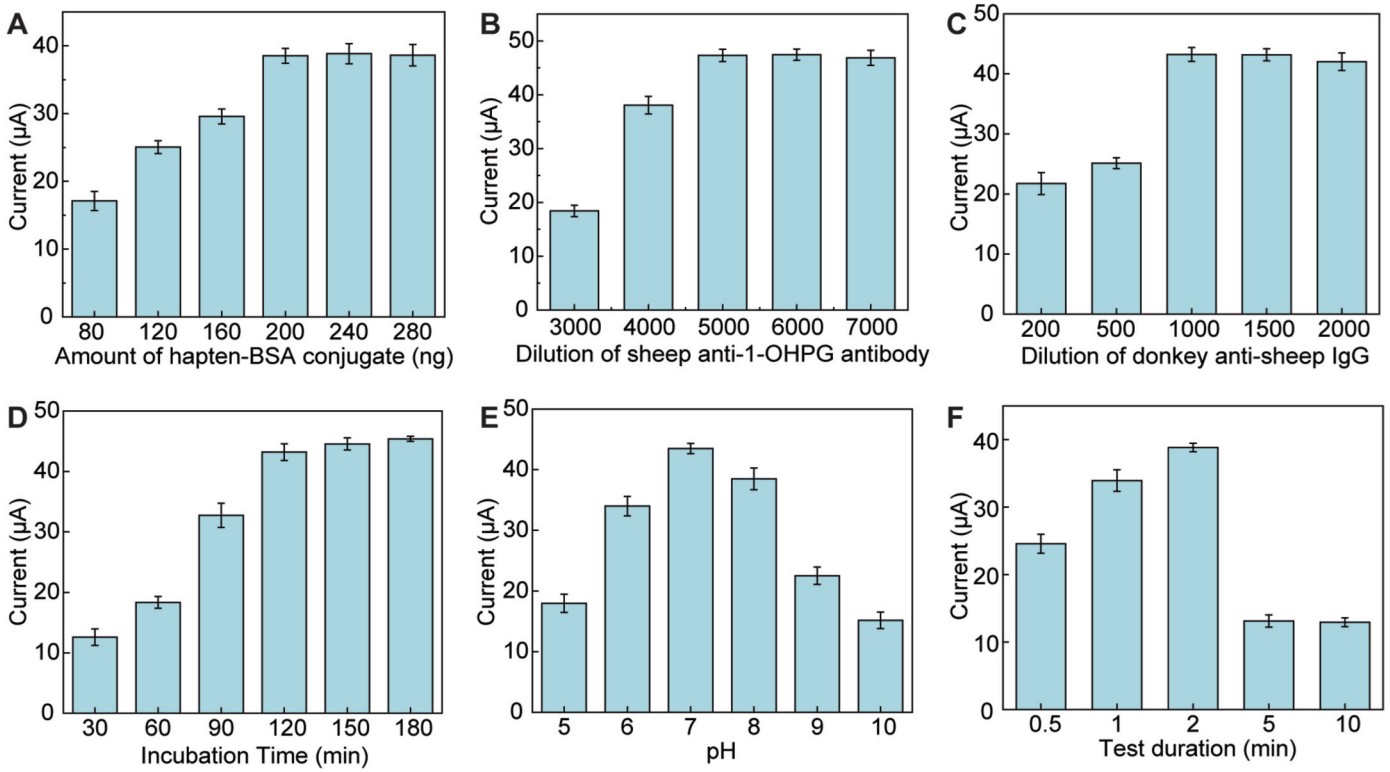

Fig. 5. Optimization of 1-OHPG immunoassay conditions. (A) Effect of the amount of hapten-BSA conjugates immobilized on the electrode surface. (B) Effect of the dilution of sheep polyclonal anti-1-OHPG Ab. (C) Effect of the dilution of donkey anti-sheep IgG. (D) Effect of incubation time. (E) Effect of buffer pH. (F) Effect of test duration on electrochemical output. Error bars represent standard deviation from three independent replicates.

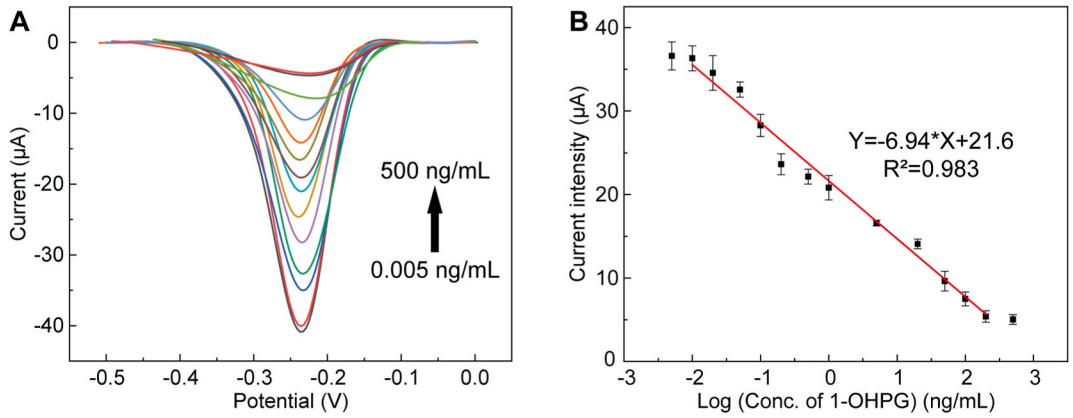

Fig. 6. The detection performance of 3D-printed 1-OHPG biosensor. (A) DPV curves at different 1-OHPG concentrations (from bottom to top: 0.005, 0.01, 0.02, 0.05, 0.1, 0.2, 0.5, 1, 5, 20, 50, 100, 200 and 500 ng/mL). (B) The calibration curve for 1-OHPG detection. Error bars represent standard deviation from three independent replicates.

immobilization on the electrode surface, improving the efficiency of antigen–antibody interactions and enhancing electrochemical signal response. To verify the stability of the 1-OHPG biosensors, the biosensors were stored at 4 °C for 1, 3, 5, 7, and 14 days. The current responses are shown in Fig. S2. After two weeks of storage, a signal retention of 91.26% was observed, demonstrating good storage stability and stable detection performance over the two-week storage. To investigate the detection performance of 1-OHPG biosensor, 1-OHPG-spiked human urine samples were analyzed to calculate recovery. The results of the spiked recovery tests are presented in Table 1. Five concentrations of 1-OHPG (100, 50, 10, 1, and 0.1 ng/mL) were spiked into human urine samples. The recovery rate ranged from 95% to 105%, with the relative standard deviation (RSD) being below 10%. These results demonstrate the feasibility and analytical reliability of the 3D-printed 1-OHPG biosensor for quantitative detection in complex biological matrices.

The detection range and LOD of various 1-OHPG detection approaches are summarized in Table 2. As shown, conventional approaches such as LC-MS/MS, GC/MS, and HPLC are widely used for 1-OHPG quantification [20,73,74]. However, these techniques often require complex sample pretreatment steps, such as elution, filtration and extraction which limit their suitability for rapid and cost-effective analysis [14,75]. In contrast, the biosensor developed in this study provides a simplified detection procedure with a significantly lower cost. It demonstrates a wide linear detection range that exceeds that of traditional methods, along with a low LOD and a stable recovery comparable to traditional analytical techniques. Lateral flow immunoassay has also been reported for urinary 1-hydroxypyrene glucuronide detection, with a detection range of 1–10 μg/L using smartphone-based signal analysis [76]. However, smartphone-based image analysis can be susceptible to ambient light and environmental conditions. In comparison, the proposed electrochemical biosensor provides quantitative detection over a wider range (0.01–200 ng/mL), while maintaining portability for field applications.

Table 1
The detection performance of 3D-printed flexible electrochemical 1-OHPG biosensor in human urine spike recovery tests.

Spiked (ng/mL)	Measured concentration (ng/mL)	Recovery	RSD[a]
100	98.3	98.3%	5.34%
50	48.7	97.4%	2.61%
10	9.85	98.5%	8.75%
1	1.06	106%	3.14%
0.1	0.0952	95.2%	4.87%

[a] RSD: Relative standard deviation. RSD was obtained from three replicate measurements.

Table 2
Performance of various approaches for the detection of 1-OHPG.

Approach	Detection range	LOD	Recovery	Ref.
LC–MS/MS	0.2-100 nmol/L (0.08-40 ng/mL)	0.13 fmol/injection[a] (0.005 ng/mL)	/	[20]
UPLC-MS/MS	0.1-2.0 ng/mL	0.015 ng/mL	79.4-106%	[15]
UPLC-FLD[b]	0.01-5 ng/mL	0.0032 ng/mL	91.9-109%	[14]
GC/MS	/	0.01 ng/mL	82%	[74]
μSPE–iEESI–MS/MS[c]	0.0001–0.1 ng/L	0.02 pg/L	91–95%	[75]
SFS[d]	/	0.05 pmol/mL (0.02 ng/mL)	/	[77]
HPLC-MS/MS	/	0.015 ng/mL	/	[73]
3D-printed biosensor	0.01-200 ng/mL	0.012 ng/mL	95-105%	This work

[a] Injection volume was 10 μL.
[b] UPLC-FLD: ultra-performance liquid chromatography–fluorescence detection.
[c] μSPE–iEESI–MS/MS: micro-solid-phase extraction followed by direct detection with internal extractive electrospray ionization mass spectrometry.
[d] SFS: synchronous fluorescence spectroscopy.

4. Conclusion

In this research, we successfully developed a highly sensitive 3D-printed flexible electrochemical biosensor for the detection of 1-OHPG, exhibiting a linear detection range of 0.01–200 ng/mL and a low LOD of 0.012 ng/mL. The biosensor was fabricated using multiple 3D-printing techniques (FDM, SLA and DIW) to achieve its functions. The accuracy, reproducibility, and reliability of the biosensor were confirmed through recovery tests using 1-OHPG-spiked human urine samples, yielding recovery between 95% and 105% with an RSD ranging from 2% to 8%. The biosensor's remarkable detection performance is attributed to several synergistic factors: (1) An innovative DIW-based immobilization method that ensures uniform distribution of hapten-BSA conjugates on the electrode surface, greatly enhancing detection stability and accuracy. (2) Comprehensive electrode activation methods that significantly improve electrochemical properties and boost sensitivity. (3) A robust immunochemical reaction-based detection mechanism, leveraging specific antigen–antibody binding to achieve high selectivity and specificity. (4) An efficient hybrid 3D printing strategy that simplifies fabrication, reduces production costs, and improves manufacturing efficiency. Collectively, these strengths position this innovative biosensor as a simple, accurate, and cost-effective solution

for 1-OHPG detection in human urine, with strong potential for rapid, portable monitoring of PAH exposure. Moreover, the precise positioning and high-resolution trace deposition capabilities of the DIW technique are highly advantageous for developing biosensors that require accurate and uniform molecular immobilization on electrode surfaces. This capability enables the fabrication of sensors capable of immobilizing multiple molecules on a single miniature electrode for simultaneous, multiplexed biomarker detection, which will be an exciting focus of our future research. In addition, the flexible substrate fabricated by SLA offers excellent potential for integration into wearable sensor designs in forthcoming work.

CRediT authorship contribution statement

Yonghao Fu: Writing – original draft, Methodology, Investigation, Data curation. **Chuchu Chen:** Methodology, Investigation, Data curation. **Xinyi Li:** Writing – review & editing, Methodology, Investigation, Data curation. **Yang Song:** Methodology, Investigation. **Christopher D. Simpson:** Writing – review & editing. **Luke P. Naeher:** Writing – review & editing. **Kaiyan Qiu:** Writing – review & editing, Supervision, Methodology, Funding acquisition, Conceptualization. **Dan Du:** Writing – review & editing, Supervision, Methodology, Funding acquisition, Conceptualization.

Declaration of competing interest

The authors declare that they have no known competing financial interests or personal relationships that could have appeared to influence the work reported in this paper.

Acknowledgments

This work was supported by the Centers for Disease Control and Prevention/National Institute for Occupational Safety and Health, CDC/NIOSH) Grant No. 1 R01OH012579-01-00. Its contents are solely the responsibility of the authors and do not necessarily represent the official views of CDC. This work was also supported by Startup Funds and Commercialization Special Project Funds from Washington State University.

Appendix A. Supplementary data

Supplementary data to this article can be found online at https://doi.org/10.1016/j.talanta.2026.129778.

Data availability

Data will be made available on request.

References

[1] M. Burke, A. Driscoll, S. Heft-Neal, J. Xue, J. Burney, M. Wara, The changing risk and burden of wildfire in the United States, Proc. Natl. Acad. Sci. 118 (2021) e2011048118, https://doi.org/10.1073/pnas.2011048118.
[2] X. Huang, K. Ding, J. Liu, Z. Wang, R. Tang, L. Xue, et al., Smoke-weather interaction affects extreme wildfires in diverse coastal regions, Science 379 (2023) 457–461, https://doi.org/10.1126/science.add9843.
[3] NIFC, Wildfires and Acres | National Interagency Fire Center, National Interagency Fire Center, 2024. https://www.nifc.gov/fire-information/statistics/wildfires.
[4] O. Adetona, C.D. Simpson, Z. Li, A. Sjodin, A.M. Calafat, L.P. Naeher, Hydroxylated polycyclic aromatic hydrocarbons as biomarkers of exposure to wood smoke in wildland firefighters, J. Expo. Sci. Environ. Epidemiol. 27 (2017) 78–83, https://doi.org/10.1038/jes.2015.75.
[5] A.M. Paiva, B. Barros, M. Oliveira, S. Alves, F. Esteves, A. Fernandes, et al., Biomonitoring of polycyclic aromatic hydrocarbons exposure and short-time health effects in wildland firefighters during real-life fire events, Sci. Total Environ. 926 (2024) 171801, https://doi.org/10.1016/j.scitotenv.2024.171801.
[6] H. Jin, W. Yuan, W. Li, J. Yang, Z. Zhou, L. Zhao, et al., Combustion chemistry of aromatic hydrocarbons, Prog. Energy Combust. Sci. 96 (2023) 101076, https://doi.org/10.1016/j.pecs.2023.101076.
[7] I. Chan, S.R. Schneider, A. Cheng, S.A. Styler, Wildfire smoke contributions to polycyclic aromatic hydrocarbon loadings in Western Canadian urban surface grime, Environmental Science & Technology 59 (2025) 2745–2753, https://doi.org/10.1021/acs.est.4c09630.
[8] A.B. Patel, S. Shaikh, K.R. Jain, C. Desai, D. Madamwar, Polycyclic aromatic hydrocarbons: sources, toxicity, and remediation approaches, Front. Microbiol. 11 (2020) 562813, https://doi.org/10.3389/fmicb.2020.562813.
[9] J.L.R. Baum, U. Bakali, C. Killawala, K.M. Santiago, E. Dikici, E.N. Kobetz, et al., Evaluation of silicone-based wristbands as passive sampling systems using PAHs as an exposure proxy for carcinogen monitoring in firefighters: evidence from the firefighter cancer initiative, Ecotoxicol. Environ. Saf. 205 (2020) 111100, https://doi.org/10.1016/j.ecoenv.2020.111100.
[10] M. Oliveira, K. Slezakova, M.J. Alves, A. Fernandes, J.P. Teixeira, C. Delerue-Matos, et al., Polycyclic aromatic hydrocarbons at fire stations: firefighters' exposure monitoring and biomonitoring, and assessment of the contribution to total internal dose, J. Hazard Mater. 323 (2017) 184–194, https://doi.org/10.1016/j.jhazmat.2016.03.012.
[11] Y. Fu, Y. Song, Z. Yang, X. Ruan, Y. Lin, D. Du, Rapid and sensitive detection of wood smoke exposure biomarkers using europium fluorescent nanoparticle label/lateral flow immunoassay, Talanta 291 (2025) 127760, https://doi.org/10.1016/j.talanta.2025.127760.
[12] F. Dehghani, F. Omidi, O. Heravizadeh, S. Yousefinejad, Solidified floating organic droplet microextraction coupled with HPLC for rapid determination of trans, trans muconic acid in benzene biomonitoring, Sci. Rep. 11 (2021) 15751, https://doi.org/10.1038/s41598-021-95174-5.
[13] Z.M. Karazan, M. Roushani, A new method for electrochemical determination of hippuric acid based on molecularly imprinted copolymer, Talanta 246 (2022) 123491, https://doi.org/10.1016/j.talanta.2022.123491.
[14] M. Yang, Y. Wang, J. Ren, M. Li, Q. Wang, N. Li, et al., A rapid and sensitive method of determination of 1-Hydroxypyrene glucuronide in urine by UPLC–FLD, Chromatographia 82 (2019) 835–842, https://doi.org/10.1007/s10337-019-03713-0.
[15] M. Li, Q. Wang, J. Zhu, N. Li, X. Zou, A simple analytical method of determining 1-hydroxypyrene glucuronide in human urine by isotope dilution with ultra performance liquid chromatography-tandem mass spectrometry, Anal. Bioanal. Chem. 409 (2017) 1513–1518, https://doi.org/10.1007/s00216-016-0083-y.
[16] P. Jacob, M. Wilson, N.L. Benowitz, Determination of phenolic metabolites of polycyclic aromatic hydrocarbons in human urine as their pentafluorobenzyl ether derivatives using liquid chromatography– tandem mass spectrometry, Anal. Chem. 79 (2007) 587–598, https://doi.org/10.1021/ac060920l.
[17] G. Gmeiner, C. Krassnig, E. Schmid, H. Tausch, Fast screening method for the profile analysis of polycyclic aromatic hydrocarbon metabolites in urine using derivatisation–solid-phase microextraction, J. Chromatogr. B Biomed. Sci. Appl. 705 (1998) 132–138, https://doi.org/10.1016/S0378-4347(97)00526-4.
[18] Y. Li, A.C. Li, H. Shi, S. Zhou, W.Z. Shou, X. Jiang, et al., The use of chemical derivatization to enhance liquid chromatography/tandem mass spectrometric determination of 1-hydroxypyrene, a biomarker for polycyclic aromatic hydrocarbons in human urine, Rapid Commun. Mass Spectrom. 19 (2005) 3331–3338, https://doi.org/10.1002/rcm.2196.
[19] J. Brandi, G. Siragusa, E. Robotti, E. Marengo, D. Cecconi, Analysis of veterinary drugs and pesticides in food using liquid chromatography-mass spectrometry, TrAC, Trends Anal. Chem. 179 (2024) 117888, https://doi.org/10.1016/j.trac.2024.117888.
[20] K. Kakimoto, A. Toriba, T. Ohno, M. Ueno, T. Kameda, N. Tang, et al., Direct measurement of the glucuronide conjugate of 1-hydroxypyrene in human urine by using liquid chromatography with tandem mass spectrometry, J. Chromatogr. B 867 (2008) 259–263, https://doi.org/10.1016/j.jchromb.2008.04.015.
[21] R. Singh, M. Tuček, K. Maxa, T. Jana, E.H. Weyand, A rapid and simple method for the analysis of 1-hydroxypyrene glucuronide: a potential biomarker for poly cyclic aromatic hydrocarbon exposure, Carcinogenesis 16 (1995) 2909–2915, https://doi.org/10.1093/carcin/16.12.2909.
[22] A.H. Ali, High-performance liquid chromatography (HPLC): a review, Annal. Adv. Chem. (2022), https://doi.org/10.29328/journal.aac.1001026.
[23] R.R.A. Soares, R.G. Hjort, C.C. Pola, K. Parate, E.L. Reis, N.F.F. Soares, et al., Laser-induced graphene electrochemical immunosensors for rapid and label-free monitoring of Salmonella enterica in chicken broth, ACS Sens. 5 (2020) 1900–1911, https://doi.org/10.1021/acssensors.9b02345.
[24] S. Jafari, M. Dehghani, N. Nasirizadeh, M.H. Baghersad, M. Azimzadeh, Label-free electrochemical detection of cloxacillin antibiotic in milk samples based on molecularly imprinted polymer and graphene oxide-gold nanocomposite, Measurement 145 (2019) 22–29, https://doi.org/10.1016/j.measurement.2019.05.068.
[25] P. Singh, S.K. Pandey, J. Singh, S. Srivastava, S. Sachan, S.K. Singh, Biomedical perspective of electrochemical nanobiosensor, Nano-Micro Lett. 8 (2016) 193–203, https://doi.org/10.1007/s40820-015-0077-x.
[26] O.-M. Istrate, L. Rotariu, C. Bala, Amperometric L-Lactate biosensor based upon a gold nanoparticles/reduced graphene oxide/polyallylamine hydrochloride modified screen-printed graphite electrode, Chemosensors 9 (2021) 74, https://doi.org/10.3390/chemosensors9040074.
[27] F. Cui, H. Jafarishad, Z. Zhou, J. Chen, J. Shao, Q. Wen, et al., Batch fabrication of electrochemical sensors on a glycol-modified polyethylene terephthalate-based microfluidic device, Biosens. Bioelectron. 167 (2020) 112521, https://doi.org/10.1016/j.bios.2020.112521.
[28] C. Chen, Y. Fu, Y. Liu, Y. Lin, D. Du, K. Qiu, 3D-printed biocompatible hollow microneedle-based electrochemical sensor for wireless glucose monitoring, ChemRxiv (2025), https://doi.org/10.26434/chemrxiv-2025-gv8xt.

[29] X. Ruan, Y. Wang, E.Y. Kwon, L. Wang, N. Cheng, X. Niu, et al., Nanomaterial-enhanced 3D-printed sensor platform for simultaneous detection of atrazine and acetochlor, Biosens. Bioelectron. 184 (2021) 113238, https://doi.org/10.1016/j.bios.2021.113238.
[30] M. Ding, S. Ding, D. Du, X. Wang, X. Hu, P. Guan, et al., Recent advances in electrochemical biosensors for the detection of Aβ42, a biomarker for alzheimer disease diagnosis, TrAC, Trends Anal. Chem. 164 (2023) 117087, https://doi.org/10.1016/j.trac.2023.117087.
[31] S. Ding, S. Li, Z. Lyu, J. Zhou, S. Tang, L. Fang, et al., Single-atom materials boosting wearable orthogonal uric acid detection, Med-X 2 (2024) 12, https://doi.org/10.1007/s44258-024-00027-1.
[32] S. Nesaei, Y. Song, Y. Wang, X. Ruan, D. Du, A. Gozen, et al., Micro additive manufacturing of glucose biosensors: a feasibility study, Anal. Chim. Acta 1043 (2018) 142–149, https://doi.org/10.1016/j.aca.2018.09.012.
[33] S. Ding, Z. Lyu, S. Li, X. Ruan, M. Fei, Y. Zhou, et al., Molecularly imprinted polypyrrole nanotubes based electrochemical sensor for glyphosate detection, Biosens. Bioelectron. 191 (2021) 113434, https://doi.org/10.1016/j.bios.2021.113434.
[34] M. Parrilla, A. Sena-Torralba, A. Steijlen, S. Morais, Á. Maquieira, K. De Wael, A 3D-printed hollow microneedle-based electrochemical sensing device for in situ plant health monitoring, Biosens. Bioelectron. 251 (2024) 116131, https://doi.org/10.1016/j.bios.2024.116131.
[35] R.M. Cardoso, C. Kalinke, R.G. Rocha, P.L. Dos Santos, D.P. Rocha, P.R. Oliveira, et al., Additive-manufactured (3D-printed) electrochemical sensors: a critical review, Anal. Chim. Acta 1118 (2020) 73–91, https://doi.org/10.1016/j.aca.2020.03.028.
[36] L. Zhong, X. Du, Y. Jiang, J. Wen, X. Wang, W. Shuoti, et al., N-doped graphene quantum dots and gold co-modified 3D printed electrode for sensitive detection of dopamine, Microchem. J. 212 (2025) 113432, https://doi.org/10.1016/j.microc.2025.113432.
[37] H. Yang, M. Liao, J. Ou, Y. Yang, L. Zhong, Y. Jiang, et al., Copper-decorated covalent organic framework covalently modified 3D-printed nanocarbon electrodes for the determination of methotrexate, Microchem. J. 207 (2024) 111886, https://doi.org/10.1016/j.microc.2024.111886.
[38] M. McCole, M. Bradley, M. McCaul, D. McCrudden, A low-cost portable system for on-site detection of soil pH and potassium levels using 3D printed sensors, Results Eng. 20 (2023) 101564, https://doi.org/10.1016/j.rineng.2023.101564.
[39] M.A. Ali, C. Hu, E.A. Yttri, R. Panat, Recent advances in 3D printing of biomedical sensing devices, Adv. Funct. Mater. 32 (2022) 2107671, https://doi.org/10.1002/adfm.202107671.
[40] B. Li, S. Zhang, L. Zhang, Y. Gao, F. Xuan, Strain sensing behavior of FDM 3D printed carbon black filled TPU with periodic configurations and flexible substrates, J. Manuf. Process. 74 (2022) 283–295, https://doi.org/10.1016/j.jmapro.2021.12.020.
[41] C. Chen, Y. Fu, S.S. Sparks, Z. Lyu, A. Pradhan, S. Ding, et al., 3D-Printed flexible microfluidic health monitor for in situ sweat analysis and biomarker detection, ACS Sens. 9 (2024) 3212–3223, https://doi.org/10.1021/acssensors.4c00528.
[42] C. Chen, Y. Fu, Y. Liu, P. Dutta, Y. Lin, D. Du, et al., Next-generation health monitoring: the role of nanomaterials in 3D-printed wearable devices, Mater. Today (2025), https://doi.org/10.1016/j.mattod.2025.03.005.
[43] X. Ruan, Y. Wang, N. Cheng, X. Niu, Y.-C. Chang, L. Li, et al., Emerging applications of additive manufacturing in biosensors and bioanalytical devices, Adv. Mater. Technol. 5 (2020) 2000171, https://doi.org/10.1002/admt.202000171.
[44] A. Abdalla, B.A. Patel, 3D printed electrochemical sensors, Annu. Rev. Anal. Chem. 14 (2021) 47–63, https://doi.org/10.1146/annurev-anchem-091120-093659.
[45] M.H. Omar, K.A. Razak, M.N. Ab Wahab, H.H. Hamzah, Recent progress of conductive 3D-printed electrodes based upon polymers/carbon nanomaterials using a fused deposition modelling (FDM) method as emerging electrochemical sensing devices, RSC Adv. 11 (2021) 16557–16571, https://doi.org/10.1039/D1RA01987B.
[46] V.A.O.P. Silva, W.S. Fernandes-Junior, D.P. Rocha, J.S. Stefano, R.A.A. Munoz, J. A. Bonacin, et al., 3D-printed reduced graphene oxide/polylactic acid electrodes: a new prototyped platform for sensing and biosensing applications, Biosens. Bioelectron. 170 (2020) 112684, https://doi.org/10.1016/j.bios.2020.112684.
[47] H.H. Bin Hamzah, O. Keattch, D. Covill, B.A. Patel, The effects of printing orientation on the electrochemical behaviour of 3D printed acrylonitrile butadiene styrene (ABS)/carbon black electrodes, Sci. Rep. 8 (2018) 9135, https://doi.org/10.1038/s41598-018-27188-5.
[48] T.W. von Zuben, J.R. Camargo, R.G. Rocha, P.L. dos Santos, E.M. Richter, B. C. Janegitz, et al., Advances and the growing role of additive manufacturing in the development of 3D-printed electrochemical sensors, Electrochim. Acta 543 (2025) 147566, https://doi.org/10.1016/j.electacta.2025.147566.
[49] D. Wang, R. Wang, S. Chen, J. Gao, C. Cai, Y. Zheng, et al., Low viscosity and highly flexible stereolithographic 3D printing resins for flexible sensors, Mater. Des. 243 (2024) 113052, https://doi.org/10.1016/j.matdes.2024.113052.
[50] E.S. Chen, A. Ahmadianshalchi, S.S. Sparks, C. Chen, A. Deshwal, J.R. Doppa, et al., Machine learning enabled design and optimization for 3D-Printing of high-fidelity presurgical organ models, Adv. Mater. Technol. 10 (2025) 2400037, https://doi.org/10.1002/admt.202400037.
[51] T.P. Patil, V.S. Parkhe, S.S. Kundale, R.K. Kamat, T.D. Dongale, R.S. Patil, et al., Antisense oligonucleotide conjugated gold nanoconstructs-based electrochemical biosensor for detection of SARS-CoV-2, Appl. Surf. Sci. Adv. 22 (2024) 100618, https://doi.org/10.1016/j.apsadv.2024.100618.
[52] A. Zarei, A. Hatefi-Mehrjardi, M.A. Karimi, A. Mohadesi, Impedimetric glucose biosensing based on drop-cast of porous graphene, nafion, ferrocene, and glucose oxidase biocomposite optimized by central composite design, J. Electroanal. Chem. 919 (2022) 116544, https://doi.org/10.1016/j.jelechem.2022.116544.
[53] E. Vaněčková, M. Bouša, Š.N. Lachmanová, J. Rathouský, M. Gal, T. Sebechlebská, et al., 3D printed polylactic acid/carbon black electrodes with nearly ideal electrochemical behaviour, J. Electroanal. Chem. 857 (2020) 113745, https://doi.org/10.1016/j.jelechem.2019.113745.
[54] M.P. Browne, F. Novotny, Z.k. Sofer, M. Pumera, 3D printed graphene electrodes' electrochemical activation, ACS Appl. Mater. Interfaces 10 (2018) 40294–40301, https://doi.org/10.1021/acsami.8b14701.
[55] Q. Wang, H. Wang, P. Du, J. Liu, D. Liu, P.J.E.A. Liu, Porous polylactic acid/carbon nanotubes/polyaniline composite film as flexible free-standing electrode for supercapacitors, Electrochim. Acta 294 (2019) 312–324, https://doi.org/10.1016/j.electacta.2018.10.108.
[56] C.L. Manzanares Palenzuela, F. Novotný, P. Krupička, Z.k. Sofer, M. Pumera, 3D-printed graphene/polylactic acid electrodes promise high sensitivity in electroanalysis, Anal. Chem. 90 (2018) 5753–5757, https://doi.org/10.1021/acs.analchem.8b00083.
[57] M. Abbasi, P. Váz, J. Silva, P. Martins, Head-to-Head evaluation of FDM and SLA in additive manufacturing: performance, cost, and environmental perspectives, Appl. Sci. 15 (2025), https://doi.org/10.3390/app15042245.
[58] M. Deka, N. Sinha, R. Das, N.K. Hazarika, H. Das, B. Daurai, et al., A review on the surface modification of materials for 3D-printed diagnostic devices, Anal. Methods 16 (2024) 485–495, https://doi.org/10.1039/D3AY01742G.
[59] M.S. Carvalho, R.G. Rocha, A.B. Nascimento, D.A.G. Araújo, T.R.L.C. Paixão, O. F. Lopes, et al., Enhanced electrochemical performance of 3D-printed electrodes via blue-laser irradiation and (electro)chemical treatment, Electrochim. Acta 506 (2024) 144995, https://doi.org/10.1016/j.electacta.2024.144995.
[60] Y. Chang, F. Liu, D. Xie, F. Lv, D. Wang, Z. Tian, et al., Additive manufacturing of wearable flexible sensors based on GN/flexible resin composite materials, J. Mater. Sci. 59 (2024) 11381–11392, https://doi.org/10.1007/s10853-024-09835-7.
[61] R.C. Dawkins, D. Wen, J.N. Hart, M. Vepsäläinen, A screen-printed Ag/AgCl reference electrode with long-term stability for electroanalytical applications, Electrochim. Acta 393 (2021) 139043, https://doi.org/10.1016/j.electacta.2021.139043.
[62] M.A.S.R. Saadi, A. Maguire, N.T. Pottackal, M.S.H. Thakur, M.M. Ikram, A.J. Hart, et al., Direct ink writing: a 3D printing technology for diverse materials, Adv. Mater. 34 (2022) 2108855, https://doi.org/10.1002/adma.202108855.
[63] C. Kalinke, N.V. Neumsteir, G. de Oliveira Aparecido, T.V. de Barros Ferraz, P. L. Dos Santos, B.C. Janegitz, et al., Comparison of activation processes for 3D printed PLA-graphene electrodes: electrochemical properties and application for sensing of dopamine, Analyst 145 (2020) 1207–1218, https://doi.org/10.1039/C9AN01926J.
[64] D.M. Wirth, M.J. Sheaff, J.V. Waldman, M.P. Symcox, H.D. Whitehead, J.D. Sharp, et al., Electrolysis activation of fused-filament-fabrication 3D-Printed electrodes for electrochemical and spectroelectrochemical analysis, Anal. Chem. 91 (2019) 5553–5557, https://doi.org/10.1021/acs.analchem.9b01331.
[65] E.M. Richter, D.P. Rocha, R.M. Cardoso, E.M. Keefe, C.W. Foster, R.A.A. Munoz, et al., Complete additively manufactured (3D-Printed) electrochemical sensing platform, Anal. Chem. 91 (2019) 12844–12851, https://doi.org/10.1021/acs.analchem.9b02573.
[66] Y. Wang, H. Li, B. Cui, X. Xu, Y. Wang, Simple mixed-acid-treated carbon Fiber electrodes with oxygen-containing functional groups for flexible supercapacitors, J. Compos. Sci. 7 (2023), https://doi.org/10.3390/jcs7060231.
[67] Z. Liu, D. Ye, R. Chen, B. Zhang, X. Zhu, Q. Liao, A dual-functional three-dimensional herringbone-like electrode for a membraneless microfluidic fuel cell, J. Power Sources 438 (2019) 227058, https://doi.org/10.1016/j.jpowsour.2019.227058.
[68] J.F.S. Pereira, R.G. Rocha, S.V.F. Castro, A.F. João, P.H.S. Borges, D.P. Rocha, et al., Reactive oxygen plasma treatment of 3D-printed carbon electrodes towards high-performance electrochemical sensors, Sensor. Actuator. B Chem. 347 (2021) 130651, https://doi.org/10.1016/j.snb.2021.130651.
[69] A.V. Papavasileiou, L. Děkanovský, L. Chacko, B. Wu, J. Luxa, J. Regner, et al., Unraveling the versatility of carbon Black – polylactic acid (CB/PLA) 3D-Printed electrodes via sustainable electrochemical activation, Small Methods, n/a (2025) 2402214, https://doi.org/10.1002/smtd.202402214.
[70] J.-H. Shin, K.-D. Seo, H. Park, D.-S. Park, Performance improvement of acid pretreated 3D-printing composite for the heavy metal ions analysis, Electroanalysis 33 (2021) 1707–1714, https://doi.org/10.1002/elan.202100077.
[71] D. Zhang, Y. Bai, H. Niu, L. Chen, J. Xiao, Q. Guo, et al., Enzyme immobilization by inkjet printing on reagentless biosensors for electrochemical phosphate detection, Biosensors 14 (2024) 168, https://doi.org/10.3390/bios14040168.
[72] D. Mampallil, H.B. Eral, A review on suppression and utilization of the coffee-ring effect, Adv. Colloid Interface Sci. 252 (2018) 38–54, https://doi.org/10.1016/j.cis.2017.12.008.
[73] J. Zhu, X. Zhao, M. Yang, B. Zheng, C. Sun, X. Zou, et al., Levels of urinary metabolites of benzene compounds, trichloroethylene, and polycyclic aromatic hydrocarbons and their correlations with socioeconomic, demographic, dietary factors among pregnant women in six cities of China, Environ. Sci. Pollut. Control Ser. 29 (2022) 6278–6293, https://doi.org/10.1007/s11356-021-16030-7.
[74] K.-H. Lee, R. Vermeulen, V. Lenters, S.-H. Cho, P.T. Strickland, D. Kang, Determinants of urinary 1-hydroxypyrene glucuronide in South Korean children, Int. Arch. Occup. Environ. Health 82 (2009) 961–968, https://doi.org/10.1007/s00420-008-0385-2.
[75] J. Han, W. Liu, R. Su, L. Zhu, D. Wu, J. Xu, et al., Coupling of micro-solid-phase extraction and internal extractive electrospray ionization mass spectrometry for ultra-sensitive detection of 1-hydroxypyrene and papaverine in human urine

samples, Anal. Bioanal. Chem. 411 (2019) 3281–3290, https://doi.org/10.1007/s00216-019-01794-2.

[76] L. Ball, H. Carter, C. Baker, R. Porter, The development of rapid immunoassays for the urinary analysis of 1-hydroxypyrene glucuronide facilitate both laboratory and on-site polycyclic aromatic hydrocarbon biomonitoring, Toxicol. Lett. 401 (2024) 116–124, https://doi.org/10.1016/j.toxlet.2024.10.002.

[77] R.B. Gunier, P. Reynolds, S.E. Hurley, S. Yerabati, A. Hertz, P. Strickland, et al., Estimating exposure to polycyclic aromatic hydrocarbons: a comparison of survey, biological monitoring, and geographic information system–based methods, Cancer Epidemiol. Biomark. Prev. 15 (2006) 1376–1381, https://doi.org/10.1158/1055-9965.EPI-05-0799.